

**Supplementary Material**

**Submicron Spatial Resolution in Thermal Desorption Mass Spectrometry via Rapid  
Heating using Thermal AFM Probes**

Suhas Somnath<sup>§</sup>, Stephen Jesse<sup>§</sup>, Gary J. Van Berkel<sup>#</sup>, Sergei V. Kalinin<sup>§</sup>, and Olga S.  
Ovchinnikova<sup>1§</sup>

<sup>§</sup>The Institute for Functional Imaging of Materials and the Center for Nanophase Materials  
Sciences, Oak Ridge National Laboratory, Oak Ridge, TN 37831, USA.

<sup>#</sup>Mass Spectrometry and Laser Spectroscopy Group, Chemical Sciences Division, Oak Ridge  
National Laboratory, Oak Ridge, TN 37831, USA.

Notice: This manuscript has been authored by UT-Battelle, LLC, under Contract No. DE-AC0500OR22725 with the U.S. Department of Energy. The United States Government retains and the publisher, by accepting the article for publication, acknowledges that the United States Government retains a non-exclusive, paid-up, irrevocable, world-wide license to publish or reproduce the published form of this manuscript, or allow others to do so, for the United States Government purposes. The Department of Energy will provide public access to these results of federally sponsored research in accordance with the DOE Public Access Plan (<http://energy.gov/downloads/doe-public-access-plan>).

---

<sup>1</sup> Corresponding author, [ovchinnikovo@ornl.gov](mailto:ovchinnikovo@ornl.gov)

## Governing equations for the finite difference model:

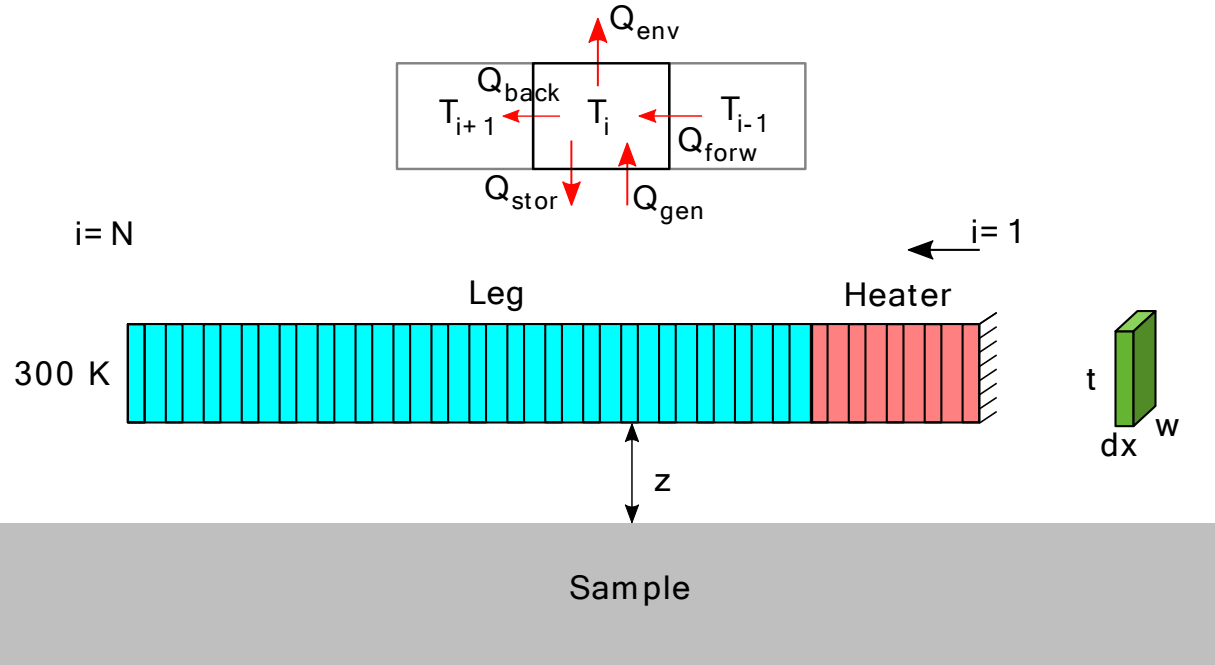


Figure S1: Schematic of the finite difference model describing the cantilever heat flow to its surroundings. The cantilever is split along the line of symmetry and modeled as a one-dimensional fin. Parameters pertaining to the cantilever width,  $w$ , cantilever thickness,  $t$ , distance between the cantilever and the sample,  $z$  are shown. Each node is of size  $t * dx * w$ . Temperature is measured at the center of each node. The first node ( $i=1$ ) is a half-node at the plane of symmetry or the center of the heater and has an adiabatic boundary condition. The last node ( $i=N$ ) is a half-node at the base of the cantilever and the temperature of this node is always 300 K due to the isothermal boundary condition. Each  $i^{\text{th}}$  node has an inward conductive heat flow from the previous ( $i-1$ ) node ( $Q_{forw}$ ), an outward conductive heat flow to the next ( $i+1$ ) node ( $Q_{back}$ ), and an outward heat flow to the environment ( $Q_{env}$ ). The volumetric heat generation ( $Q_{gen}$ ) and heat storage ( $Q_{stor}$ ) are represented as inward and outward heat flows from the node respectively.

A shape factor is used to summarize the heat flow from each cantilever node to the surrounding air and the sample.

Constants to help in simplifying or abbreviating long equations below:

$$B = \frac{2.8\Delta x * w}{z + t} k_{air} \quad (1)$$

$$A = \frac{k_{Si}(T_i)w * t}{\Delta x} \quad (2)$$

$$S = \frac{\rho_{Si} C_{Si} w * t * \Delta x}{\Delta t} \quad (3)$$

$$R_i = \rho(N_D, T_i) * \frac{\Delta x}{t * w} \quad (4)$$

$N_D$  = the number of boron dopant atoms per unit volume in single crystal silicon. This serves as the doping concentration in silicon.

$\rho$  = Electrical resistivity

$T_i$  = temperature of that node

$k_{Si}$  = thermal conductivity of silicon

$k_{air}$  = thermal conductivity of air

The different heat flows out of each node as shown in figure S1:

$$Q_{env} = \frac{2.8 \Delta x * w}{z + t} k_{air} (T_i^p - T_{env}) = B(T_i^p - T_{env}) \quad (5)$$

$$Q_{forw} = k_{Si} w * t \frac{(T_{i-1}^p - T_i^p)}{\Delta x} = A(T_{i-1}^p - T_i^p) \quad (6)$$

$$Q_{back} = k_{Si} w * t \frac{(T_i^p - T_{i+1}^p)}{\Delta x} = A(T_i^p - T_{i+1}^p) \quad (7)$$

$$Q_{stor} = \rho_{Si} C_{Si} w * t * \Delta x \frac{(T_i^{p+1} - T_i^p)}{\Delta t} = S(T_i^{p+1} - T_i^p) \quad (8)$$

$$Q_{gen} = I^2 R_i \quad (9)$$

Energy balance at each node:

$$Q_{gen} + Q_{forw} = Q_{back} + Q_{env} + Q_{stor} \quad (10)$$

Substituting (5-9) into (10):

$$I^2 R_i + A(T_{i-1}^p - T_i^p) = A(T_i^p - T_{i+1}^p) + B(T_i^p - T_{env}) + S(T_i^{p+1} - T_i^p) \quad (11)$$

Regrouping terms in (11):

$$T_i^{p+1} = \frac{1}{S} [(I^2 R_i + B * T_{env}) + (A) T_{i-1}^p + (-B - 2A + S) T_i^p + (A) T_{i+1}^p] \quad (12)$$

Subscripts will be applied to the constants defined in (1-4) to signify whether the node is a heater node or leg node since the width of the nodes are different at the heater and the cantilever legs.

Special cases:

Special node 1 - Half node at the end of the heater / line of symmetry:

Equations (10) and (12) become:

$$I^2 R_i = A_H(T_i^p - T_{i+1}^p) + \frac{B_H}{2}(T_i^p - T_{env}) + \frac{S_H}{2}(T_i^{p+1} - T_i^p) \quad (13)$$

$$T_i^{p+1} = \frac{2}{S_H} \left[ I^2 R_i + \frac{B_H}{2} T_{env} \right] + \left( -\frac{B_H}{2} - A_H + \frac{S_H}{2} \right) T_i^p + (A_H) T_{i+1}^p \quad (14)$$

Special node 2 – Half node at the base of the cantilever leg is always at room temperature due to the boundary condition:

$$T_N = T_{Env} \quad (15)$$

Special node 3 – Interface node between the heater and the leg:  
Equations (10) and (12) become:

$$I^2 R_i + A_H(T_{i-1}^p - T_i^p) = A_L(T_i^p - T_{i+1}^p) + \left\{ \frac{B_H + B_L}{2} \right\} (T_i^p - T_{env}) + \left\{ \frac{S_H + S_L}{2} \right\} (T_i^{p+1} - T_i^p) \quad (16)$$

$$\begin{aligned} T_i^{p+1} &= \frac{2}{S_H + S_L} \left[ I^2 R_i + \left\{ \frac{B_H + B_L}{2} \right\} T_{env} \right] + (A_H) T_{i-1}^p + \left( -\left\{ \frac{B_H + B_L}{2} \right\} - A_H - A_L + \frac{S_H}{2} \right) T_i^p + (A_L) T_{i+1}^p \end{aligned} \quad (17)$$

When implementing the implicit solver, equations (12), (14), and (17) are rewritten as:

$$-(A) T_{i-1}^{p+1} + (B + 2A + S) T_i^{p+1} - (A) T_{i+1}^{p+1} = (I^2 R_i + B) T_{env} + S T_i^p \quad (18)$$

$$0 * T_{i-1}^{p+1} + \left( \frac{B_H}{2} + A_H + \frac{S_H}{2} \right) T_i^{p+1} - (A_H) T_{i+1}^{p+1} = (I^2 R_i + \frac{B_H}{2}) T_{env} + \frac{S_H}{2} T_i^p \quad (19)$$

$$\begin{aligned} -(A_H) T_{i-1}^{p+1} + (B_{mean} + A_H + A_L + S_{mean}) T_i^{p+1} - (A_L) T_{i+1}^{p+1} \\ = (I^2 R_i + B_{mean}) T_{env} + S_{mean} T_i^p \end{aligned} \quad (20)$$

Where:

$$B_{mean} = \left\{ \frac{B_H + B_L}{2} \right\}; \quad S_{mean} = \left\{ \frac{S_H + S_L}{2} \right\} \quad (21)$$

Equations (15), (18-20) are arranged in a matrix format and solved as follows. Configuration for the generic node as well as the three special nodes are shown.:



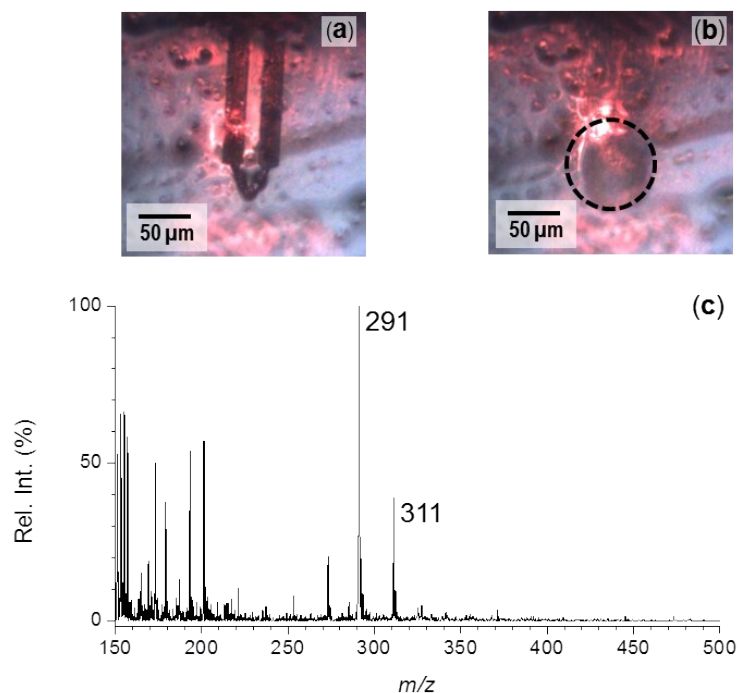


Figure S3. Thermal damage of low melting point candelilla wax matrix containing UV-stabilizers avobenzone and oxinoxate. Optical photograph of candelilla wax surface (a) prior to heating and (b) post heating at 300 °C for 1 s directly on the surface. (c) Background subtracted full scan mass spectrum from heating event in panel b. Background spectrum was taken when tip was heating at 300 °C and not engaged on the surface. The cantilever was heated with scheme I.

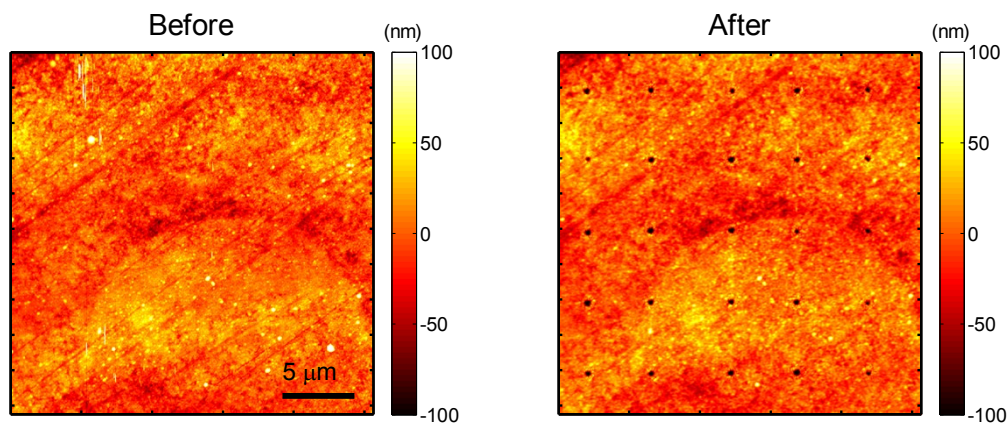


Figure S4: Sample topography before and after a set of MS-TD experiments using heating scheme IV. The topography scans show that the topography before and after the experiments is virtually identical with the exception of the desorption craters. Redeposition and reflow of the sample material is not visible for this heating scheme.

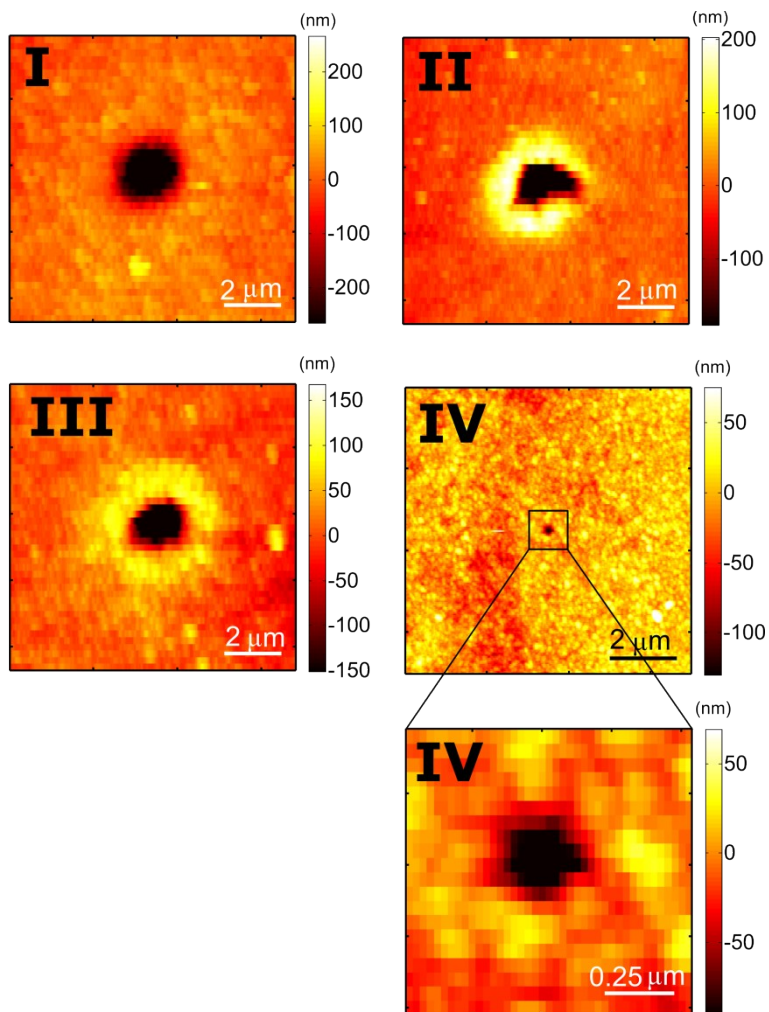


Figure S5: Sample topography after AFM-TD-MS experiments using four heating schemes (I, II, III, and IV). Scheme IV results in the smallest desorption craters.

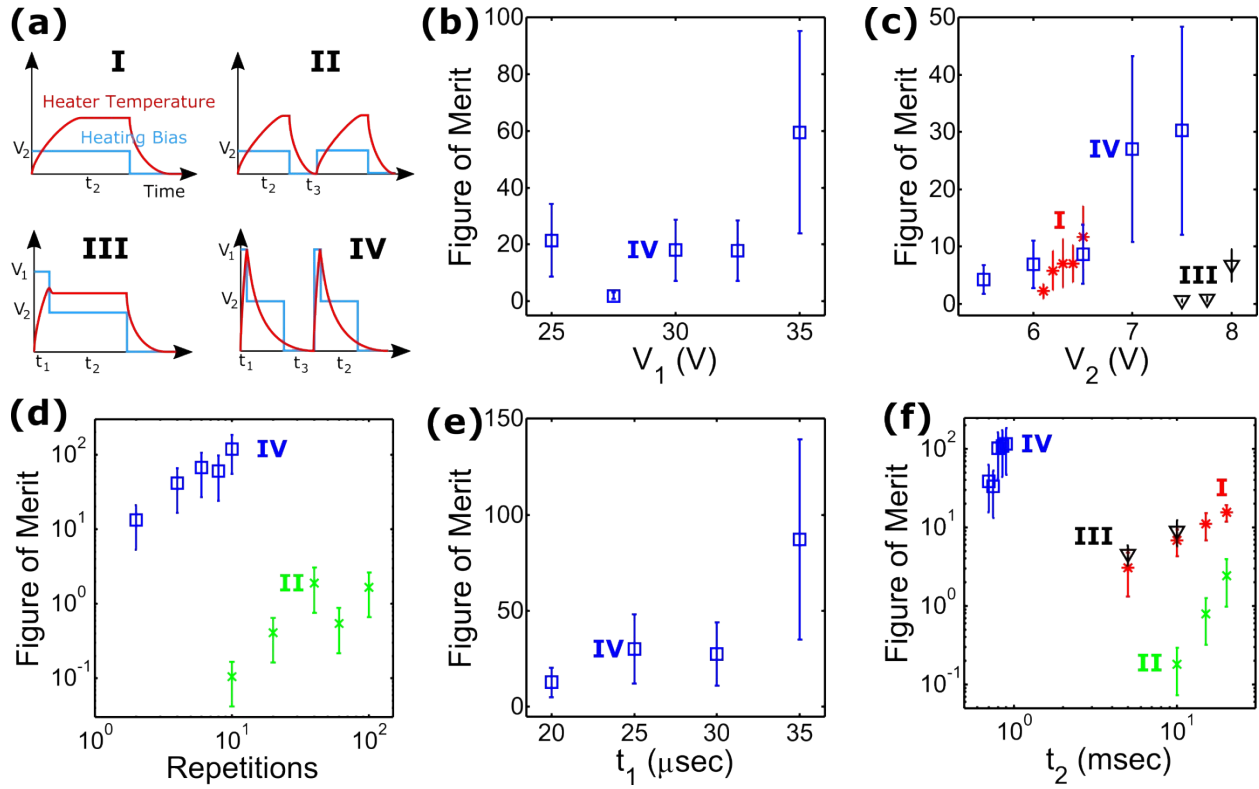


Figure S6. (a) Schematic of the heater temperature and heating bias of the four heating schemes. An additional figure of merit can be defined as the quotient of the mass spectral signal and the diameter of the effective spot size. The effective spot size takes the reflow and re-deposition of sample material into account. (b-f) The figure-of-merit as a function of the different heating voltages ( $V_1$ ,  $V_2$ ), heating durations ( $t_1$ ,  $t_2$ ), and heating-pulse repetitions. The figure-of-merit is defined as the quotient of the mass spectrometer signal and the desorption crater diameter. In descending order of their figure of merits, the heating schemes can be arranged as IV, I, III, and II.

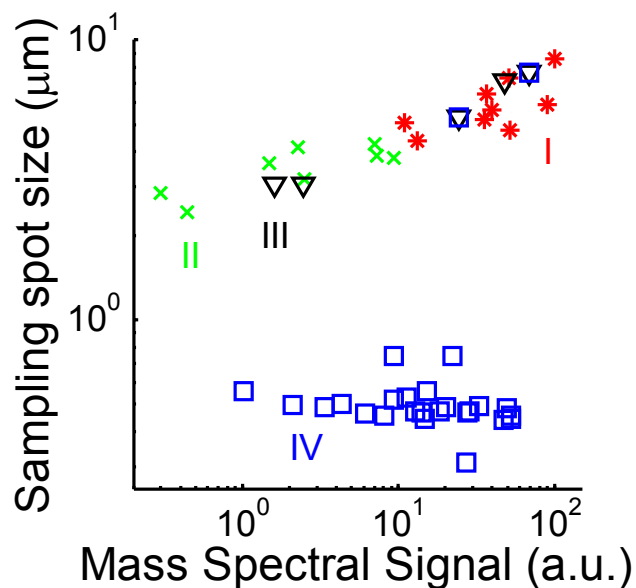


Figure S7. Mean sampling spot size as a function of mean mass spectral signal for all heating schemes. The sampling spot size here takes the sample reflow and re-deposition diameters into account where appropriate. These are the fundamental measurable quantities in all experiments. The goal of this study is to minimize the spot size while maintaining sufficiently high mass spectral signals. Thus points on the lower right section of the above are most desirable while those on the top left section are least desirable. Clearly, scheme II performs the worst while the performance of scheme I and III can be said to be comparable. Scheme IV clearly achieves the best performance metric. These findings are very similar to those found in Figure 4(f).

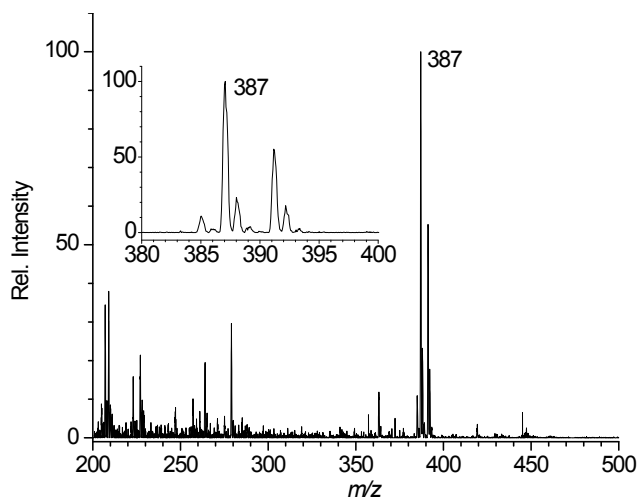


Figure S8. TD/SI-MS background subtracted full scan mass spectrum of yellow ink on premium photo paper. Insert shows the zoomed in region around the main component of the yellow ink.

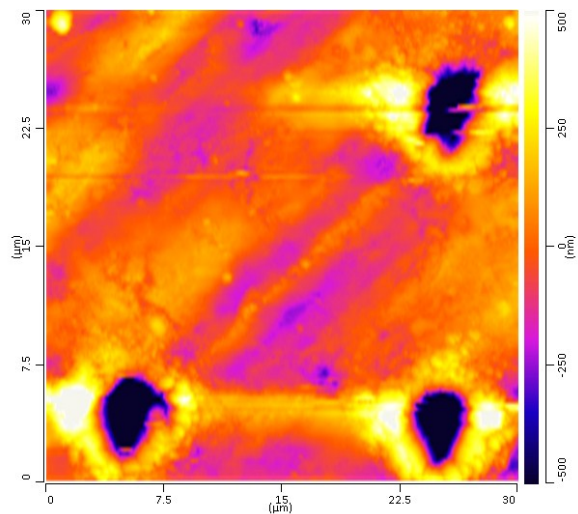


Figure S9. AFM topography images of a rubrene pellet showing three desorption craters surrounded by significant reflow and redeposition.